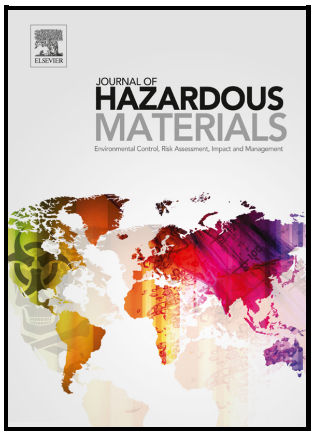
Journal Pre-proof



Acid Mine Drainage and Waste Dispersion in Legacy Mining Sites: An Integrated Approach using UAV Photogrammetry and Geospatial Analysis

Ana Barroso, Renato Henriques, Ângela Cerqueira, Patrícia Gomes, Isabel Margarida Horta Ribeiro Antunes, Amélia Paula Marinho Reis, Teresa Maria Valente

PII: S0304-3894(25)01743-1

DOI: https://doi.org/10.1016/j.jhazmat.2025.138827

Reference: HAZMAT138827

To appear in: *Journal of Hazardous Materials*

Received date: 23 March 2025
Revised date: 7 May 2025
Accepted date: 2 June 2025

Please cite this article as: Ana Barroso, Renato Henriques, Ângela Cerqueira, Patrícia Gomes, Isabel Margarida Horta Ribeiro Antunes, Amélia Paula Marinho Reis and Teresa Maria Valente, Acid Mine Drainage and Waste Dispersion in Legacy Mining Sites: An Integrated Approach using UAV Photogrammetry and Geospatial Analysis, *Journal of Hazardous Materials,* (2025) doi:https://doi.org/10.1016/j.jhazmat.2025.138827

This is a PDF file of an article that has undergone enhancements after acceptance, such as the addition of a cover page and metadata, and formatting for readability, but it is not yet the definitive version of record. This version will undergo additional copyediting, typesetting and review before it is published in its final form, but we are providing this version to give early visibility of the article. Please note that, during the production process, errors may be discovered which could affect the content, and all legal disclaimers that apply to the journal pertain.

Journal Pre-proof

Acid Mine Drainage and Waste Dispersion in Legacy Mining Sites: An Integrated Approach using UAV Photogrammetry and Geospatial Analysis

[1]Ana Barroso, [1]Renato Henriques, [1]Ângela Cerqueira, [1]Patrícia Gomes, [1]Isabel Margarida Horta Ribeiro Antunes, [1,2]Amélia Paula Marinho Reis, [1]Teresa Maria Valente

[1]Universidade do Minho, Campus de Gualtar, Institute of Earth Sciences, 710-057 Braga, Portugal;

[2]GEOBIOTEC, Geosciences Department, University of Aveiro, Campus Universitário de Santiago, 3810-193 Aveiro, Portugal

Corresponding author email address: id9873@alunos.uminho.pt

Abstract:

Abandoned mines pose environmental risks due to the accumulation of sulfide-rich waste, which generates acid mine drainage and and produces fine-grained, unconsolidated materials that, when deposited on steep slopes, accelerate erosion and contaminant transport. This study assesses the environmental impact of the Trimpancho mining complex by integrating UAV-based photogrammetry, water analysis, and mine waste characterization. Aerial surveys produced high-resolution orthomosaics and digital surface models, enabling the identification of runoff patterns, erosion hotspots, and waste accumulation. The estimated waste volume is approximately 253,377 m^3.

Key findings highlight critical erosion areas on steep slopes (>30°) where waste mobilization enhances metal and sulfate transport into the Trimpancho stream, affecting the Chança River. Water samples have pH values ranging from 2.59 to 8.27, electrical conductivity peaking at 4,171 µS/cm, and elevated concentrations of iron (65.7 mg/L), aluminum (174 mg/L), manganese (23.5 mg/L), and zinc (20.7 mg/L). Mine waste characterization revealed that Nuestra Señora del Carmen dump exhibited higher leaching potential compared to Volta Falsa.

This study underscores the value of UAV technology for cost-effective and high-resolution environmental monitoring in abandoned mines. The results emphasize the need for targeted remediation strategies and water quality improvement. This multi method approach can serve as a model for assessing contamination risks and optimizing environmental monitoring programs in other legacy mining sites.

Environmental implication:

This study highlights the severe environmental impacts of abandoned mine waste in the Iberian Pyrite Belt. High sulfide content and steep slopes contribute to acid mine drainage, contaminating downstream water bodies, including the Chança River. UAV-based photogrammetry combined with hydrochemical data revealed critical hotspots for contaminant mobilization. These insights are essential for prioritizing remediation strategies and guiding sustainable management of legacy mining sites, especially in transboundary water systems at risk.

Keywords: remote sensing, environmental monitoring, IPB, waste assessment, erosion dynamics

Highlights:

- AMD confirmed, with pH as low as 2.59 and high metal concentrations and loads.
- Erosion hotspots on slopes >30° increase metal transport to water bodies.
- NSC dump shows higher leaching potential than VF, mainly slag and oxides.
- UAV Photogrammetry enables high-resolution mapping of waste and drainage patterns.

- Multi-method approach enhances monitoring, highlighting priority areas for AMD mitigation.

Journal Pre-proof

Graphical abstract:



Journal Pre-proof

1. Introduction

Abandoned mining sites pose severe environmental challenges, particularly in regions with a long history of mining activity (Doumas et al., 2018). One such example is the Iberian Pyrite Belt (IPB), one of the world's largest volcanogenic massive sulfide (VMS) provinces, which has been extensively mined from prehistoric times to the late 20th century (Tornos et al., 2000; Nocete et al., 2005). As a result, more than 100 mines in the IPB have been abandoned (León et al., 2021), leaving behind vast amounts of sulfide-rich waste. Historically, only a small fraction of the extracted ore was recovered for valuable metals, with over 90% of the material discarded as waste (Cánovas et al., 2021). The absence of proper environmental regulations at the time further exacerbated contamination risks, leading to widespread pollution and long-term ecological damage.

A major environmental consequence of abandoned sulfide-rich waste is the formation of acid mine drainage (AMD) (Helser et al., 2022). When exposed to oxygen and water, sulfide minerals oxidize, producing highly acidic leachate enriched in dissolved metals and sulfate. This acidification severely impacts surrounding surface waters, groundwater, and sediments, degrading ecosystems and posing risks to human health (Hoffert, 1947; Nordstrom, 2011). The prolonged environmental impact is compounded by ongoing oxidation and metal leaching, which continue for decades after mining operations cease (España et al., 2005; González et al., 2018; Olías et al., 2020; Cánovas et al., 2023; Gomes & Valente, 2024).

In addition to AMD, erosion and waste dispersion further deteriorate abandoned mining landscapes. Unregulated disposal of mine waste results in runoff-driven erosion, destabilizing waste piles and transporting contaminated sediments into watercourses (Silva et al., 2005). Erosion channels in steep terrains accelerate material loss, exacerbating AMD effects by increasing sedimentation in nearby streams and rivers (Carabassa et al., 2021). Monitoring and quantifying these processes are crucial for assessing contaminant mobility, hydrological impacts, and long-term environmental risks.

Traditional monitoring methods in abandoned mining areas often face significant logistical, financial, and safety constraints, particularly in regions with rugged terrain and limited accessibility. These challenges are especially acute in the IPB, where steep slopes, unstable waste deposits, and remote locations frequently hinder the implementation of conventional fieldwork. In this context, Unmanned Aerial Vehicles (UAVs) have emerged as a transformative tool for environmental monitoring, offering flexible and rapid data acquisition with high spatial resolution (Jakob et al. 2017; Park & Choi, 2020; Dang & Nguyen, 2023), often surpassing the capabilities of aircraft or satellite-based systems (Flores et al., 2021). UAV-based photogrammetry enables detailed surface modelling with centimetric precision, supporting accurate assessments of erosion patterns, waste volumes, and landscape changes (Padró et al., 2022; Alsayed & Nabawy, 2023; Nogueira et al., 2023).

In mining contexts, UAVs have been widely used for applications such as open-pit mapping, tailings dam monitoring, post-mining rehabilitation assessment, and the mapping of AMD-affected areas (Hämmerle et al., 2016; Jackisch et al., 2018; Rauhala et al., 2017; Tong et al., 2015; Keatley et al., 2018; Xiang et al., 2018; Cara et al., 2013). However, in the IPB, most UAV-based studies to date have relied primarily on hyperspectral or multispectral sensors to identify mineralogical indicators of contamination (Quental et al., 2020; Isgró et al., 2022b; Moreno González et al., 2024). By contrast, few works have integrated UAV-derived topographic data with geochemical and hydrological analysis to investigate AMD processes and waste dispersion in detail.

This study focuses on the Trimpancho mining complex, an abandoned site in the Spanish sector of the IPB, a representative but under-studied site. The research integrates UAV photogrammetry with water quality analysis and mine waste characterization to assess

contamination dispersion, AMD formation, and erosion dynamics. The main objectives are to: (i) evaluate contamination patterns by analyzing water quality along the Trimpancho stream and its connection to the Chança River; (ii) characterize mine waste in terms of mineral composition, reactivity, and leaching potential; (iii) assess erosion and sediment transport using UAV-based topographic models; (iv) demonstrate UAV efficiency in environmental monitoring and provide insights for sustainable management strategies. By addressing these objectives, this study contributes to improving environmental monitoring techniques and developing more effective remediation strategies for abandoned mining sites. Given the growing global concerns over water resource contamination and sustainable land management, the methodology presented here offers a scalable and field-validated approach applicable to other legacy mining regions worldwide.

2. Study area

The IPB, which extends across southwestern Portugal and Spain, is one of the largest and most significant VMS provinces worldwide (Isgró et al., 2022a; Gomes & Valente, 2024). Spanning approximately 230 km in length and 50 km in width, the IPB contains over 1,700 million tons of sulfide ore, including both mined and estimated reserves (Leistel et al., 1997). The region is renowned for its rich mineralization, with pyrite (FeS_2) being the dominant metallic mineral, along with lower quantities of sphalerite (ZnS), galena (PbS), chalcopyrite ($CuFeS_2$) and arsenopyrite (FeAsS). The sulfide deposits are hosted within a sequence of volcano-sedimentary rocks and are concentrated across three main lithological groups: the Phyllite-Quartzite Group (PQ), the Volcano-Sedimentary Complex (VSC), and the Culm Group (Carvalho, 1979; Barriga, 1990; Tornos, 2006; Inverno et al., 2015) (Figure 1A).

Mining in the IPB area dates to the Chalcolithic era and has been extensively exploited throughout history because of its rich mineral resources (Olías et al., 2016). However, the depletion of near-surface ore bodies and decreased economic opportunities had led to the closure of numerous mines. Nevertheless, the region continues to be a focal point for mineral exploration, with current efforts directed at deeper ore bodies, especially those rich in copper (Cu) and other metals, such as zinc (Zn), gold (Au), silver (Ag), and other strategic metals driven by the growing global demand for these resources. Consequently, the IPB's historical and current significance as a major VMS province makes it a critical area for geological, mining and environmental studies (e.g. Olías et al., 2004; Cánovas et al., 2016; Grande et al., 2017; Sánchez-Donoso et al., 2021; Isgró et al., 2022; Barroso et al., 2023; Parviainen et al., 2024; Gomes & Valente, 2024).

The Trimpancho mining complex (Figure 1B) is one of the abandoned areas in the IPB, located in the Huelva province (western part of the Spanish sector of the IPB). Like other abandoned mines, this site faces significant challenges related to AMD, primarily due to extensive waste areas exposed to weathering processes. Therefore, this area serves as a critical case study for environmental monitoring due to the lack of remediation following the cessation of mining operations at the end of the 20th century. Without proper containment measures, mine waste was indiscriminately dumped around the complex (Figure 1C), where it continues to release acid leachates into the Trimpancho stream, a tributary of the Chança River. The Chança River, which feeds the Chança reservoir, is a vital water source for both Portugal and Spain, supplying water for human consumption and agriculture. The mining complex includes four main abandoned mines: Nuestra Señora del Carmen (NSC), La Condesa (LC), Trimpancho Group (TG), and Volta Falsa (VF), (arranged from east to west; Figure 1B) (Grande et al., 2017). The area contains three major acidic pit lakes and numerous waste piles dispersed throughout the four sites.

The terrain in the area is characterized by an undulating topography, with elevations ranging from 115 m to 229 m. The Trimpancho stream, the primary drainage system, winds through valleys and ridges before merging with the Chança River. Steep slopes accelerate runoff and

erosion, while flatter sections in the former mining areas act as natural deposition zones, accumulating sediment and mine waste.

The climate in the area is classified as Csa according to the Köppen-Geiger system, with a hot-summer Mediterranean climate and semi-arid characteristics due to low annual rainfall (Beck et al., 2018). The region typically has an average annual rainfall of 630 mm and a mean annual temperature of 17.5°C (AEMET, http://www.aemet.es). These climate conditions exacerbate water scarcity, underscoring the necessity for the development of effective water management strategies. This interplay of runoff dynamics and erosion patterns plays a crucial role in stabilizing the mining landscape and preserving the region's water resources.

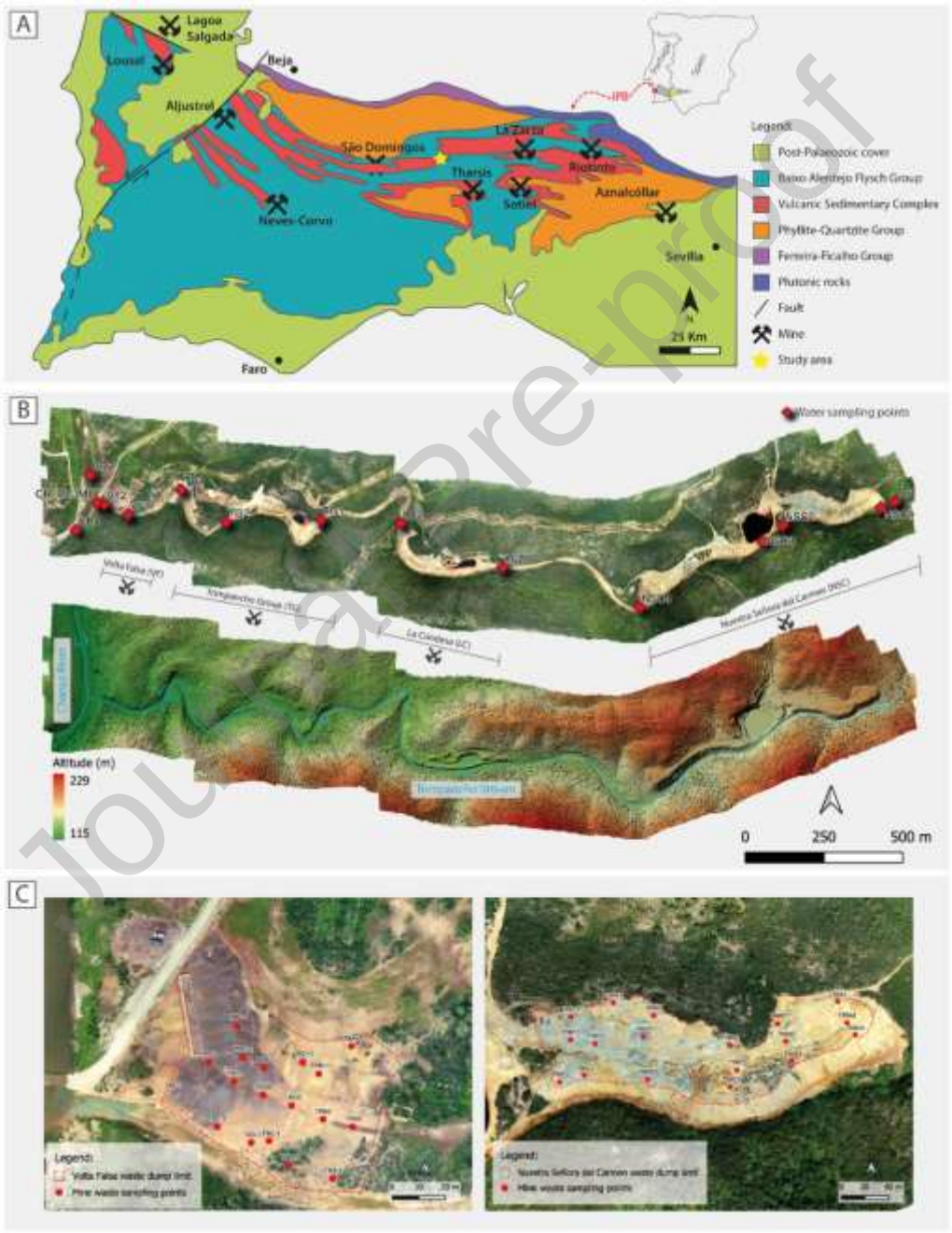


Figure 1. (A) Simplified geological map of the Iberian Pyrite Belt (IPB), highlighting the study area (adapted from Inverno et al., 2015); (B) Orthomosaic showing the water sampling locations (top) and the digital surface model (bottom) of the Trimpancho mining complex; and (C) Orthomosaic illustrating the sampling network for mine waste in the VF (left side) and NSC (right side) mine areas.

3. Material and methodology

3.1 Sampling design and field preparation

A sampling campaign was conducted during the rainy period of March 2024, aiming to capture peak leaching and contaminant transport conditions typically observed during high-flow events in AMD-affected mining areas. Surface water and mine waste samples were collected in the Trimpancho mining complex. The water samples were collected along the Trimpancho stream (Figure 1B), which receives leachate from the different waste disposal sites. A total of 15 sampling points were selected. The criterium used was to select one sample at the beginning and another at the end of each waste dump area of influence to assess the possible contribution of mine waste dump to water stream quality. In addition, water samples were also collected upstream (TS) and downstream (CR_PLUME, CR2 and CR4) of the mining complex. A water sample collected upstream of these mines was selected to represent the hydrochemical conditions without mine waste influence. Three points were selected downstream of the mines: one at the confluence of the Trimpancho stream with the Chança River, and two points in the Chança River, one before and one after the confluence area. The main objective of this sampling network was to evaluate the spatial dispersion of acid drainage along the Trimpancho and the impact of this mining system on the Chança river, since the river flows into the Chança reservoir, which is used for human consumption and agricultural irrigation.

At each sampling point, 500 mL of water was collected and stored in a sterilized polyethylene container. An aliquot of 50 mL of the sample was filtered through 0.45 μm membranes and acidified with nitric acid to a pH below 2, preventing metal precipitation and bacterial growth. All water samples were kept cool (at 4ºC) and dark conditions until laboratory analysis.

Mine waste samples were also collected to assess its reactivity and potential environmental impact. Two waste dumps were selected for analysis: NSC, located upstream of the mining complex; and VF, downstream of the mining complex. A total of 18 sampling sites were defined within each waste dump (Figure 1C), and approximately 5 kg of composite sample was collected from each site. Three waste subsamples were extracted from a depth of 10-20 cm, when feasible, and combined to form the composite sample. Waste samples were collected with a stainless-steel shovel, placed in polyethylene bags, and transported to the laboratory. The sampling network was defined randomly, with the objective of covering the largest possible area and the diversity of materials present in the highly heterogeneous waste dumps.

Furthermore, a UAV survey was conducted over the Trimpancho mining complex, utilizing a high-resolution camera to capture detailed aerial imagery. These images were processed to generate orthomosaics and digital surface models (DSMs), enabling precise mapping of waste deposits, estimation of waste volumes, and identification of environmentally degraded areas requiring closer monitoring.

3.2 Water analysis

Surface water samples were analyzed for physical and chemical properties. During the sampling process, pH, electrical conductivity (EC), and temperature (T) were measured using a multiparameter instrument (Thermo Scientific Model Orion Star A Series) with a pH electrode (Orion 9107BNM) and a conductivity cell (Orion 01310MD). Oxidation-reduction potential (ORP) was measured with an ORPTestr 10 and converted to redox potential (Eh) in accordance with the electrode characteristics. Dissolved oxygen (DO) was also measured using the HACH HQ30D portable multiparameter coupled with a dissolved oxygen probe (LDO101). Prior to analysis, all instruments were calibrated with the respective standard solutions.

Laboratory analysis was conducted for additional parameters, including acidity, alkalinity, sulfate, and metals concentrations. Acidity and alkalinity were determined by volumetric

titration (standard method 2310 B), and sulfate concentration was obtained using turbidimetry (standard method 4500-SO_4^{2-} E) (APHA, 2012) at the Department of Earth Sciences from the University of Minho (Portugal). Water concentration of metals (e.g., Fe, Al, Cu, Zn, Mn, Cd, Pb, Co, Ca, Mg, and K) were analyzed by inductively coupled plasma optical emission spectrometry (ICP-OES) in filtered and acidified aliquots. Analyses were performed at Activation Laboratory Ltd. (Actlabs, Ancaster, ON, Canada), an ISO 17025:2017 accredited and ISO 9001:2015- certified laboratory. Quality control procedures include the use of duplicate samples, blanks, and certified standards (IV-STOCK-1643) to assess analytical precision and accuracy. Detection limits varied by element, ranging from 0.01 mg/L for Fe and Mn, 0.1 mg/L for Al, K, Mg, Ca, Na, and Si, to between 2 and 10 µg/L for trace metals such as Cd, Cu, Co, Ni, Pb, and Zn. Standards solutions were Merck AA certified and Milli-Q water was used in the experiments.

3.3 Mine Waste characterization

The mine waste samples were subjected to a drying process at temperatures below 40°C, followed by disaggregation with a hammer. The samples were then homogenized and divided into quarters to obtain representative subsamples of the mine waste. Subsequently, the samples were sieved through a 2 mm sieve to remove gravel particles and separated into distinct portions for X-ray diffraction (XRD), grain size distribution, and pH/EC analysis.

A mineralogical analysis was conducted using XRD with a Philips PW 1710, APD X'pert Pro-MPD diffractometer, operating with CuK radiation and equipped with an automatic divergence slit and a graphite monochromator. Diffractograms were obtained from powders of the 2 mm fraction, spanning the range of 3 to 65° 2θ, with a 2θ step size of 0.02° and a counting time of 1.25 s. The data was processed using X'pert Pro-MPD software to the identification of mineralogical composition.

The granulometric analysis was performed using a laser diffraction particle size analyzer (Malvern Mastersizer 3000, Malvern Panalytical, UK), equipped with the Hydro LV unit. A suspension of 2 g of mine waste was prepared for analysis. Prior to analysis, three drops of sodium hexametaphosphate were added to the suspension, which was subjected to ultrasonic agitation for three minutes to ensure the disaggregation and separation of fine particles that tend to agglomerate. According to FAO (Jahn et al, 2006), the particle size was classified into the following categories: <2 µm for clay fraction, 2–50 µm for silt, and 50–2000 µm for the sand fraction.

The pH and EC of mine waste samples were determined by stirring 1 g of mine waste in 20 mL of deionized water for five minutes at 160 rpm and left still for 20-minutes to allow deposition. The pH and EC values in water suspensions were determined using a multiparameter instrument (Thermo Scientific Model Orion Star A Series), comprising a pH electrode triode and a conductivity cell. The pH electrode and conductivity cell were calibrated in accordance with the manufacturer's instructions using two buffer solutions at pH 4 and 7, and standard solutions at 147 and 1413 µS/cm, respectively.

3.4 UAV data acquisition and processing

The survey was conducted using a Phantom 4 RTK by DJI™, based in Shenzhen, Guangdong, China. The UAV covered an area approximately of 1.27 km^2, with a maximum width of 480 m and a maximum length of 2.77 km. To ensure full photogrammetric coverage of the extensive study area while accounting for the limited battery life of the Phantom 4 RTK, a total of four flights were conducted. Each flight was carried out at an altitude of 120 m, following a parallel row pattern with a 70% front overlap and 70% side overlap to optimize image alignment. MapPilot®, a flight planning application developed by Maps Made Easy™, was used to plan the mission. This software incorporates NASA's SRTM altitude models, maintaining a consistent altitude relative to the terrain, which ensures uniform Ground Sampling Distance

(GSD) across the surveyed area. The resulting photogrammetric products included a DSM and an orthomosaic, both with a GSD of 3.47 cm per pixel (Figure 1B).

Due to accessibility challenges in certain areas, only RTK (Real-Time Kinematic) corrections were applied for the positional calibration of the final cartographic products. RTK correction data was obtained in real-time from the Portuguese GNSS permanent stations network (ReNEP), specifically using the Mértola station, located at 37º 38'47.53941"N, 7º 39'36.17880"W, with an ellipsoidal altitude of 79.616 m. To ensure positional accuracy, only images with a successful real-time data flow and a positional error below 5 cm in the x, y, or z coordinates were used. While high-precision data was not a primary requirement for this study, the adopted workflow ensured survey quality equivalent to official cartographic data provided by the Portuguese Direção Geral do Território (DGT), the national authority for cartographic information. To further enhance sub-meter accuracy of the photogrammetric products, ground control points (GCPs) were incorporated using survey-grade data.

The photogrammetric processing of UAV imagery, including image mosaicking, georeferencing, orthomosaic generation, DSM creation, and 3D point cloud reconstruction, was performed using Metashape® software from Agisoft™. Agisoft Metashape, developed by Agisoft LLC (St. Petersburg, Russia), is a photogrammetry processing tool available in Standard and Pro editions. In this study, the Pro edition was used to generate 3D models from 2D aerial images and estimate mine waste volumes across the complex. The processing flow used replicates the processing used by Gonçalves & Henriques (2015), producing materials with high geodetic accuracy. These materials always showed sub-decimetric deviations when compared to the LIDAR surveys obtained from the download portal of Spain's National Cartographic Information Centre at http://centrodedescargas.cnig.es/CentroDescargas/buscadorCatalogo.do?codFamilia=LIDAR.

The most effective approach for waste volume estimation typically involves comparing DSMs before and after deposition or utilizing original topographic data (Martín-Velázquez, et al., 2022; Padró et al., 2022; Davoise & Méndez, 2023). However, since original topographic data was unavailable for this site, alternative volume estimation methods provided by Agisoft Metashape were applied (summarized in Table 1).

To enhance volume estimation accuracy, the contributions of vegetation and old mining structures within the waste dump were calculated separately and subtracted from the total estimated waste volume.

A detailed morphological analysis of the study area was conducted using the open-source GIS software, QGIS version 3.38.1. This analysis enabled a detailed analysis of the geomorphological, hydrological, and geochemical characteristics of the area. A set of geospatial processing tools was used to analyze the region's physical features and their environmental implications. Slope analysis was preformed using the "Slope raster tool", which permitted the identification of the areas with extreme gradients, which are naturally more susceptible to erosion and soil instability. These areas are of particular concern as may exacerbate environmental degradation processes. Additionally, a hydrological analysis was carried out using the "r.terraflow" module, a component of the GRASS GIS complement that is included in the processing toolbox of QGIS. This tool models the runoff patterns and the accumulation areas, providing critical insights into the water dynamics within the study area. Furthermore, a geochemical analysis was conducted through the generation of Voronoi polygons, utilizing a segmentation approach based on the influence areas of each data point in the geochemical dataset. This method facilitates the creation of geochemical maps that represent the spatial distribution of water and waste chemical properties, which are critical for understanding soil composition and potential contamination risks.

Journal Pre-proof

Table 1. Detailed description of volume calculation methods in AGISoft Metashape.

Option	Description	When to Use
Best Fit Plane	Adjusts an inclined plane automatically to minimize error in the lowest points, fitting the plane to the area of interest.	When the area exhibits a natural slope and an optimized reference plane for the mesh is required.
Mean Level Plane	Computes a horizontal plane based on the average elevation of the selected points.	When a reference plane is needed to represent the mean elevation, without considering extreme variations.
Custom Level Plane	Allows manual specification of the reference plane's height based on a predefined value or a reference point.	When a known reference level is available and should be directly applied, without automatic adjustments.

4. Results

4.1 Water properties

The statistical summary of the water physical-chemical properties is presented in Table 2. The pH values ranged from 2.59 to 8.27, with a mean of 2.92 and a median of 2.86, reflecting considerable variability and the presence of both acidic and near-neutral conditions. EC values varied between 222 to 4171 µS/cm, while sulfate concentrations ranged from 9.8 to 3359 mg/L. Eh varies between 429 to 746 mV characteristic of an oxidized environment. Among the metals analyzed, Fe, Al, and Mg exhibited the highest concentrations, with maximum levels reaching 65.7 mg/L, 174 mg/L, and 329 mg/L, respectively.

Table 2. Statistical summary of water parameters.

Parameter	Minimum	Maximum	Mean	Median	Standard-deviation
pH	2.59	8.27	2.92	2.86	2.18
EC (µS/cm)	222	4171	2254	2638	1510
DO (mg/L)	7.01	9.81	8.53	8.43	0.65
Eh (mV)	429	746	653	706	107
T (°C)	14.6	25.3	20.4	19.9	2.96
Sulfate (mg/L)	9.8	3359	1543	1817	1168
Acidity (mg/L $CaCO_3$)	713	1420	1065	1113	234
Alkalinity (mg/L $CaCO_3$)	52.7	81.0	68.9	77.6	12.8
Fe Total (mg/L)	0.02	65.7	19.6	21.7	18.0
Al (mg/L)	0.10	174	90.9	98.7	69.3
K (mg/L)	0.90	2.30	1.28	1.10	0.40
Mg (mg/L)	8.20	329	159	179	115
Mn (mg/L)	0.01	23.5	12.2	14.8	9.27
Si (mg/L)	3.90	44.7	25.4	31.7	16.4
Ca (mg/L)	11.3	98.8	54.9	70.8	32.8
Cd (µg/L)	2.00	38.0	16.4	17.0	13.7
Co (µg/L)	2.00	435	216	277	161
Cu (µg/L)	2.00	9300	4084	5430	3116
Na (mg/L)	18.3	37.0	28.7	32.7	7.22
Ni (µg/L)	5.00	307	162	200	114
Pb (µg/L)	10.0	100	30.7	10.0	27.9
Zn (µg/L)	5.00	20700	7455	4740	7777

Journal Pre-proof

Spatial variations in the hydrochemical parameters were observed across the mining complex (Figure 2). At the initial sampling sites (TS and NCS1), pH values were neutral (7.04 and 6.95, respectively). However, pH declined downstream, reaching acidic values (3.05 to 2.59) at AMD-influenced locations (NSC2 to VF2; Figure 1B). At the confluence of the Trimpancho and Chança rivers, the pH increased to 6.47, continuing to rise in the Chança River, reaching near-neutral values (8.27 upstream and 7.82 downstream of the confluence). Eh exhibited an inverse trend, with higher Eh values corresponding to lower pH. Similarly, sulfate concentration and EC increased after NSC1, varying along the stream until CR_PLUME, where both parameters sharply declined.

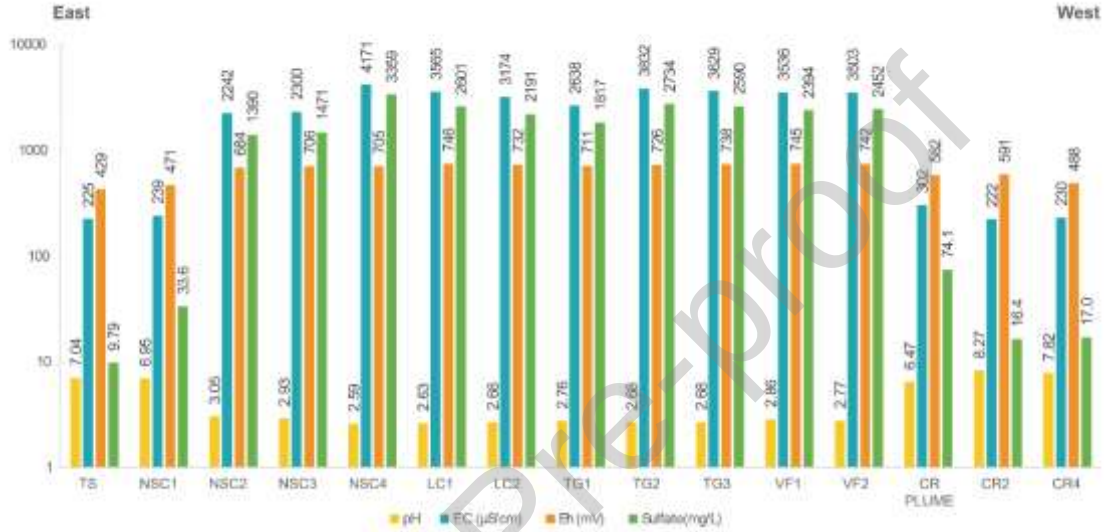


Figure 2. Spatial variation of selected water physicochemical properties.

Ficklin's diagram was used to classify water samples based on dissolved metal concentrations and pH (Ficklin et al., 1992; Figure 3). Samples collected from the Trimpancho stream, except for NSC1, were categorized as "high-acid with high metal concentrations." In contrast, TS and CR2 were classified as “near-neutral with low metal concentrations”, as they are unaffected sample points. Similarly, NCS1, CR4, and CR_PLUME fall into the same classification, likely due to mixing or dilution effects.

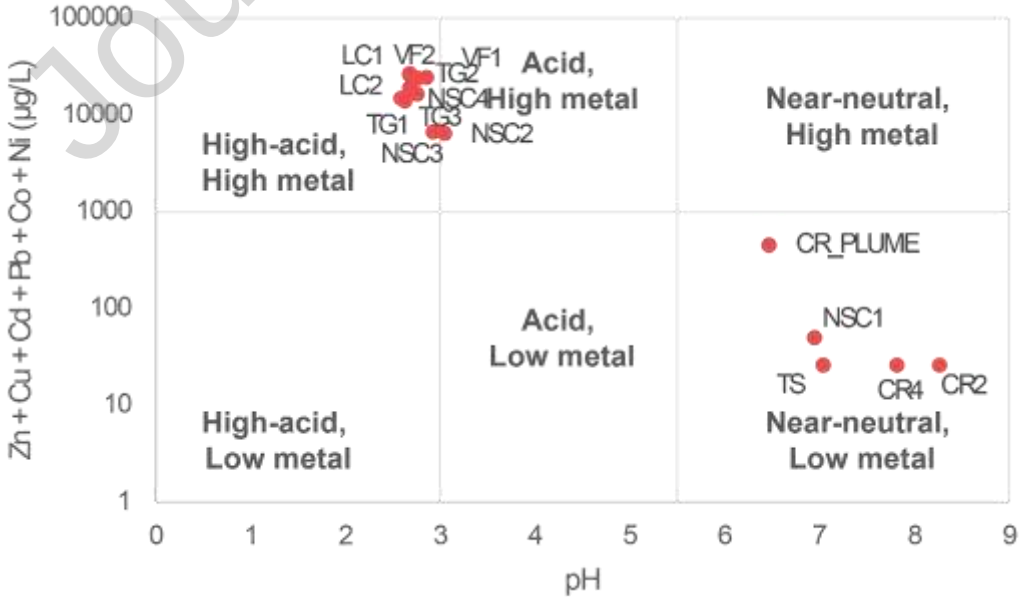


Figure 3. Projection of water samples in Ficklin diagram.

4.2 Mine wastes properties characterization

The properties of mine waste from the two waste dumps (VF and NSC) are presented in Table 3. The VF waste dump primarily consists of slag, iron oxides, and silicates, with minor sulfides. The average pH is 3.35 (ranging from 2.77 to 5.05), while EC averaged 324 µS/cm, ranging from 11.2 to 1,296 µS/cm. The waste is composed of 47% sand, 44% silt, and 9% clay, with textures varying from loam to sandy loam. The NSC waste dump exhibits higher sulfide concentrations, leading to greater acidity (mean pH = 2.69, range: 2.42 to 3.60). The mean EC is 2,063 µS/cm, reaching up to 2,920 µS/cm. The particle size distribution is 54% sand, 36% silt, and 10% clay, with similar textural classifications to the VF dump.

Table 3. Physical and chemical characteristics of mine waste from the VF (TR) and NSC (TR6) dumps.

		pH	EC (µS/cm)	Particle size			Textural Classification (FAO 2006)	Main Composition
				Clay (<2 µm)	Silt (2–50 µm)	Sand (50–2000 µm)		
VF (TR)	**Minimum**	2.77	11.2	5	19	23	Loam, Sandy loam, Silty loam, Loamy sand	Quartz, Aluminosilicates, Hematite, Goethite, Chalcopyrite, Sphalerite, Galena,
	Maximum	5.05	1296	16	62	76		
	Mean	3.35	324	9	44	47		
	Median	3.64	74	10	45	49		
	Standard-deviation	0.68	409	3	12	14		
NSC (TR6)	**Minimum**	2.42	699	3	14	26	Loam, Sandy loam, Silty loam, Loamy sand	Quartz, Aluminosilicates, Chalcopyrite, Pyrite, Copiapite, Jarosite Goethite
	Maximum	3.60	2920	14	61	83		
	Mean	2.69	2063	10	36	54		
	Median	2.74	2179	11	33	57		
	Standard-deviation	0.26	703	3	12	14		

4.3 Photogrammetric Analysis

The total estimated volume of dispersed mine waste in the Trimpancho complex is 253 377 m^3, with approximately 80% concentrated in the NSC mine site (Table 4). The waste covers a total area of 86 035 m^2 with NSC once again being the dominant contributor.

Table 4. Total areas and estimated volumes of mine waste for each mining area within the Trimpancho Mining Complex.

Mining area	Option used in AGISoft Metashape	Total area (m^2)	Volume of waste (m^3)
Nuestra Señora del Carmen mine (NSC)	Best fit plane	49 583	197 569
La Condesa mine (LC)	Best fit plane	16 097	26 501
Trimpancho group (TG)	Custom Level Plane (based on the average lower elevations along the base of the waste dump)	18 303	27 107
Volta Falsa mine (VF)	Best fit plane and Mean Level Plane	2 052	2 200
Total		86 035	253 377

Journal Pre-proof

The results obtained for the slope map of the Trimpancho mining complex, located in a steep-sided valley, show a topography characterized by a variety of slopes ranging from 0º to up to 89º (Figure 4A). The slope has a heterogeneous spatial distribution dominated by moderate to high slopes, especially along the mine waste dumps.

A closer examination of each mining area shows that in the NSC mine area, which includes two waste dumps separated by a pit lake, reveals that the outer boundaries of the waste dumps have very high slopes, exceeding 35º (indicated in red). However, the tops of the waste dumps are relatively flat. The pit lake is characterized by slopes greater than 35º (Figure 4A – NSC mine). The LC mine is characterized by high slopes (red tones, >35º), especially on the outer edges of the waste dumps and on the slope of the pit lake. The areas with lower slopes (0º to 15º) are usually located at the top of the waste dumps or in areas subject to erosion (Figure 4A – LC mine). In the TG mine, there is also a wide variation in slopes, suggesting a more irregular surface (Figure 4A – TG mine). High slopes are predominant at the edge of the waste dumps, highlighted by orange and red tones (>30°), while the upper part has smooth slopes (bluish to yellowish tones, 0°-15°). The pit lake area shows sharp slopes (>35°), marked in red tones. Finally, the VF mine has a predominance of gentle slopes, with extensive areas between 0º and 15º, shown in blue and yellow colors on the map (Figure 4A – VF mine). However, there are scattered areas of higher slopes (25º to >35º) associated with piles of loose mine waste.

In addition to slope analysis, surface runoff flows, and accumulation zones were modeled to create the flow and accumulation spatial distribution (Figure 4B). Thin blue lines represent the primary surface runoff, while dark blue zones indicate areas of water accumulation, highlighting depression zones and flow convergence patterns.

In the NSC mining area, due to the flat morphology, surface runoff is characterized by scarce accumulation zones at the top of the waste dumps. Drainage from the slopes of the waste dumps forms several water flows that converge on the main watercourse, the Trimpancho stream. The pit lake receives runoff from the waste dumps and the main escarpment, which under certain meteorological conditions will allow a drainage increase into the Trimpancho stream, as observed at the NSC3 site. Therefore, the sampling sites NSC1 to NSC4 were strategically selected to monitor runoff patterns and to assess water quality draining from the waste dumps (Figure 4B – NSC mine). The LC mining area features two primary drainage systems (Figure 4B – LC mine). The first system channels runoff from the waste dumps directly into the watercourse, transporting sediments and potential contaminants. The second system directs the surface runoff toward the pit lake, following the inner edges of the waste dumps. This runoff accumulates in a depression, ultimately feeding into the pit lake. Additionally, a small lagoon, separated from the pit lake by mine waste, has formed. This lagoon receives water inflows from the surrounding waste deposits, further contributing to localized contamination. Thus, the LC1 and LC2 sampling points were placed at accumulation areas, to monitor the transport of potential contaminants upstream and downstream of the mining area.

In the TG area, the surface runoff exhibits two primary drainage zones: one that discharges directly into the Trimpancho stream and the other into the pit lake. Drainage to the Trimpancho watercourse carries rainfall runoff and potential contaminants from the waste dumps, as evidenced by drainage marks on the escarpments (Figure 4B – TG mine). The pit lake receives drainage from multiple sources: of surface runoff from a forested area, which has minimal influence from mine waste, and flow from the reactive waste dump. As in the previous mines, water sampling was carried out in accumulation zones (TG1 to TG3), which receive runoff from the waste dump. Finally, in the VF area, the flow map displays a well-defined drainage pattern, with multiple flow paths converging toward a primary direction that consistently drains into the Trimpancho stream, with sampling at VF1 and VF2 (Figure 4B – VF mine).

Journal Pre-proof

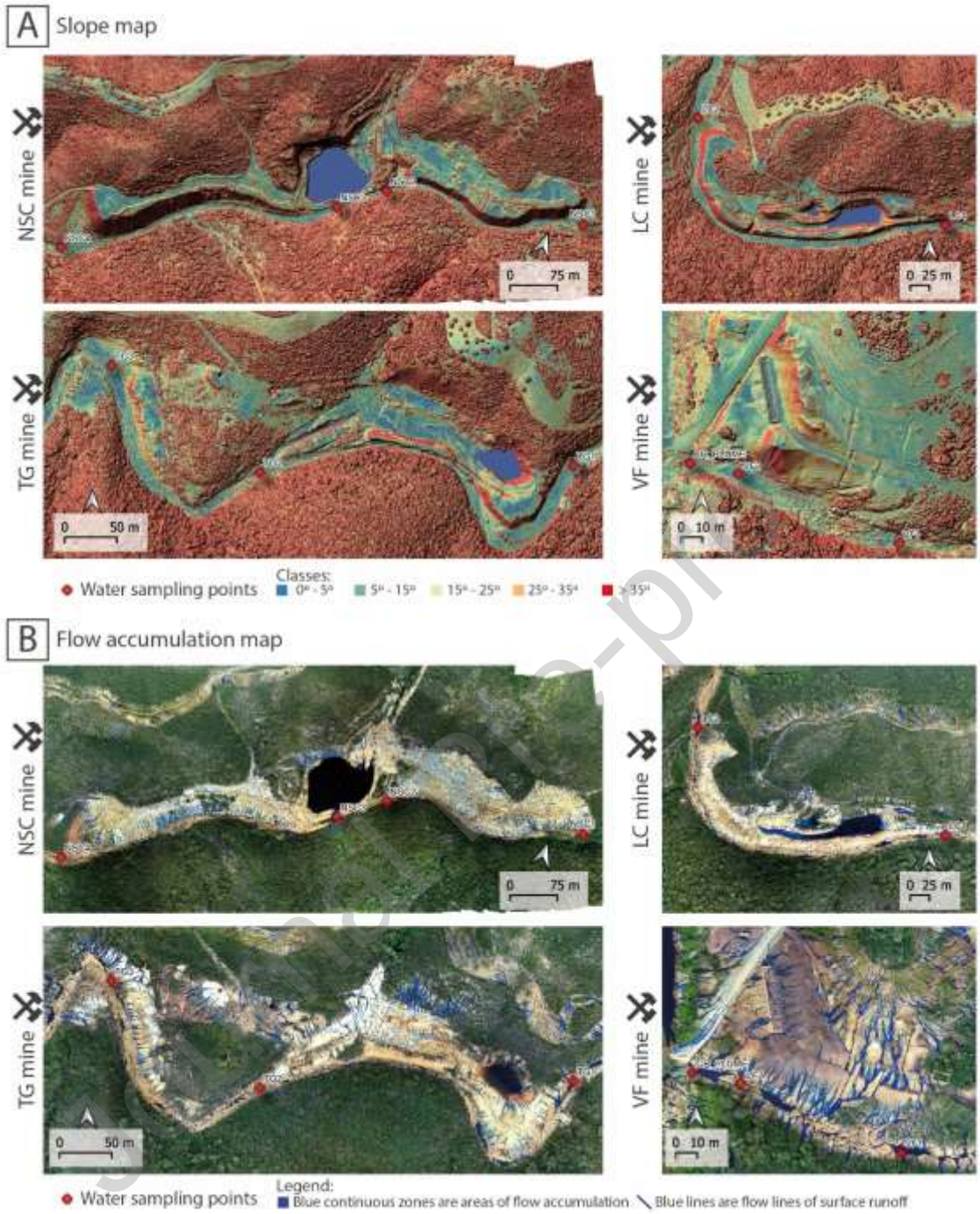


Figure 4. The slope map (A) and surface flow accumulation map (B) are superimposed on the aerial orthomosaic.

5. Discussion

The combined analysis of water and mine waste composition, integrated with data from the photogrammetric survey, enables a detailed characterization of the interactions among topography, leachate circulation, and the potential environmental impacts of unmanaged waste deposits at the Trimpancho mining complex. The integration of UAV-derived spatial data with chemical and physical measurements allows for a more comprehensive understanding of contaminant dispersion dynamics.

For instance, high-resolution DSMs generated from UAV imagery helped identify steep slopes and surface drainage pathways—key geomorphological features that influence the distribution patterns of pH, EC, and metal concentrations in surface waters. By spatially correlating these measurements with mapped terrain features, it becomes possible to directly associate contamination hotspots with erosion-prone zones, leachate flow paths, and dump configurations.

This integrated approach provides two main advantages: (1) it offers clear visual evidence of the spatial relationships between landscape and contamination, and (2) it establishes a geospatial analytical framework that enhances the interpretation of point-based water quality data within a broader environmental context.

The physical-chemical characterization of surface water collected in the Trimpancho stream shows a typical pattern of waters affected by AMD, evidenced by low pH, high EC, and relevant concentration of metals and sulfate (Nordstrom, 2011).Water samples from NSC1 to VF2 were collected in water accumulation areas that receive flow from the waste dumps (Figure 4), thereby reflecting the influence of mine waste leaching on the hydrochemical composition. The geochemical reactivity of mine waste is reflected by its physical-chemical properties, such as pH and EC. The spatial distribution of pH and EC of the NCS and VF and their consequent reactivity are represented by Voronoi polygons on the orthomosaic Figure 5. The class intervals for pH and EC were defined using the equal interval method, applied separately to the VF and NSC datasets, to represent the full range of measured values in six evenly distributed classes.

Although direct measurements of surface runoff quality were not available for each mapped polygon, pH and EC values obtained from mine waste sampling points provided valuable insight into the potential for acid generation and contaminant mobilization. When combined with the spatial distribution of water sampling points along the stream and surface flow patterns inferred from flow accumulation models, these data support the identification of relationships between waste type, geochemical reactivity, and the resulting impacts on water quality. The NSC dump, rich in sulfides, exhibited high geochemical reactivity (Figure 5 A and B), favoring AMD. This process enhances the mobilization of metals such as Fe, Al, Mn, and Zn, with relatively high concentrations observed at sampling points NSC2 to VF2. The data indicates very low pH values along the Trimpancho stream (pH<3.0) and high sulfate concentrations, reaching up to 3,359 mg/L. The high water EC values support the assumption of intense leaching processes. Additionally, the fine particle size of the NSC dump materials, composed of 10% clays and 36% silt, further facilitates metal dissolution due to the increased surface contact with water, promoting contaminant mobilization in the water system (Erguler et al., 2014; Lemos et al., 2021; Cánovas et al., 2023).

In contrast, the VF waste dump, predominantly composed of slag and iron oxides, exhibits lower reactivity, with an average pH of 3.35 and EC of 324 µS/cm (Figure 5 C and D). However, despite its lower reactivity, the influence of mine waste remains evident in the water quality samples collected along the mainstream, except at NSC1 and CR_PLUME, which are in mixing zones and where dilution effects were observed. The Ficklin's diagram's classification of water samples (Figure 3) further supports these observations. Samples collected from the Trimpancho stream, except for NSC1, were classified as "high-acid with high metal concentration". In contrast, NSC1, CR4, and CR_PLUME were classified as "near-neutral with low metal concentration", likely due to mixing or dilution effects. NSC1, located upstream of the first waste dump (Figure 1B), has a relatively lower pH (6.95) than the unaffected sampling point TS (pH 7.04), reflecting the effect of mixing fresh water with leachate from NSC waste. A similar process is observed at CR_PLUME, located at the confluence of the Trimpancho stream with the Chança River, which results in a pH increase due to dilution effects.

In addition to the reactivity of the waste, the hydrochemical characteristics of the water system are also influenced by regional geomorphology and weather conditions. These factors

are key drivers of contaminant dispersion through both surface water and wind-driven pathways (Sims et al., 2013; Doumas et al., 2018; Barroso et al., 2021), directly affecting the transport of solid waste and the mobility of associated metals from the dumps into the hydrological network. The UAV-based photogrammetric survey identified critical zones where slope gradients frequently exceed 35° (Figure 4), a condition strongly associated with increased erosion risk (Sánchez-Donoso et al., 2019; Martín-Velázquez et al., 2022).

According to Sánchez-Donoso et al. (2019), steep and unconsolidated slopes are highly susceptible to erosion features such as piping and gully formation, especially in areas with low compaction. Although compacted tailings may initially appear stable, repeated wetting and drying cycles common in semi-arid regions can gradually weaken their structure. This vulnerability is exacerbated by intense rainfall and dry summers, which favour both water and wind erosion (Doumas et al., 2018; Martín-Velázquez et al., 2022). Older tailings, typically less compact and more heterogeneous, are more prone to surface runoff, while finer and more uniform modern tailings tend to be affected by wind erosion. The absence of vegetation and protective surface layers, particularly on steep terrain, further increases erosion risk. This is consistent with field observations, such as erosion channels and waste accumulation along the watercourse, which confirm the high vulnerability of these materials to mobilization.

The spatial variation of pH, EC, Eh, and sulfate concentrations along the watercourse (Figure 2) are in good agreement with the observed runoff patterns. Surface runoff accumulations coincide with steep waste deposits, significantly contributing to contaminant dispersion. The Trimpancho stream exhibits a progressive decrease in pH, increasing EC and sulfate concentrations downstream, further enhancing the influence of mine waste leachates. However, the sharp decrease in EC and sulfate concentrations at CR_PLUME suggests a dilution effect due to the confluence with the Chança River, referred earlier, demonstrating the interplay between hydrology and contaminant transport.

The instability of waste dumps in these areas can also lead to landslides and partial collapses, exacerbating metal mobilization into the water system. Additionally, the relationship between steep slopes, erosion hotspots, and surface drainage intensity is critical in material transport rates, accelerating the leaching of metals like Fe, Al, and Mn. The accumulation of contaminated sediments along the watercourse, caused by surface runoff, contributes to the enduring degradation of the Trimpancho stream and the contamination of the Chança River. The extent of this impact was estimated by calculating the contaminant load carried into the Chança River. This estimation was based on the concentration of dissolved metals in surface water, the surface area of each waste dump, and the average annual precipitation in the region (Ostalé, 2014; Fortes et al., 2021). By combining these variables, it is possible to obtain an approximate value (in kg/year) for the contaminants in analysis, that could be mobilized through rainfall-driven leaching processes (Figure 6). Although simplified, this method provides a useful first-order indication of contaminant release potential, particularly in abandoned mine sites where direct flow measurements are often unavailable.

The four mining areas contribute differently to the overall load to the mainstream, influenced by factors such as waste volume, geochemical composition, and location within the hydrographic network. The NSC mine, located upstream and containing the largest volume of waste (197 569 m^3), is the primary source of contamination with the highest annual loads of sulfate (1.05×10^5 kg), Al (5.40×10^3 kg), and Fe (2.05×10^3 kg). Significant amounts of Mn (7.34×10^2 kg), Cu (2.91×10^2 kg), Ni (9.59×10^0 kg), and Cd (6.87×10^{-1} kg) are also detected, reflecting the high sulfide content and reactivity of the waste. The LC mine (26 501 m^3) has lower but important contamination levels, contributing 2.22×10^4 kg of sulfate, with Al (1.29×10^3 kg), Fe (2.60×10^2 kg) and Mn (1.86×10^2 kg) as the dominant metals. Cu (7.64×10^1 kg), Ni (2.30×10^0 kg) and Cd (2.23×10^{-1} kg) are also present. The TG mine, with a similar waste volume (27 107 m^3), presents

comparable values: sulfate (2.99×10^{4} kg), Al (2.01×10^{3} kg), Fe (2.79×10^{2} kg) and Mn (2.50×10^{2} kg) are most prominent, followed by Cu (6.57×10^{1} kg), Ni (3.12×10^{0} kg) and Cd (4.27×10^{-1} kg).

Finally, VF2, which is located downstream and has the smallest waste volume (2 200 m^3), has the lowest contamination load, with sulfate (3.17×10^{3} kg), Al (1.90×10^{2} kg), Fe (2.80×10^{1} kg), and Mn (2.51×10^{1} kg) as the main contributors. Cu (7.37×10^{0} kg), Ni (3.06×10^{-1} kg), and Cd (4.27×10^{-2} kg) are significantly lower. Despite its lower individual contribution, VF2 still plays a role in cumulative downstream contamination, with persistent metal and sulfate inputs to the Chança River.

Journal Pre-proof

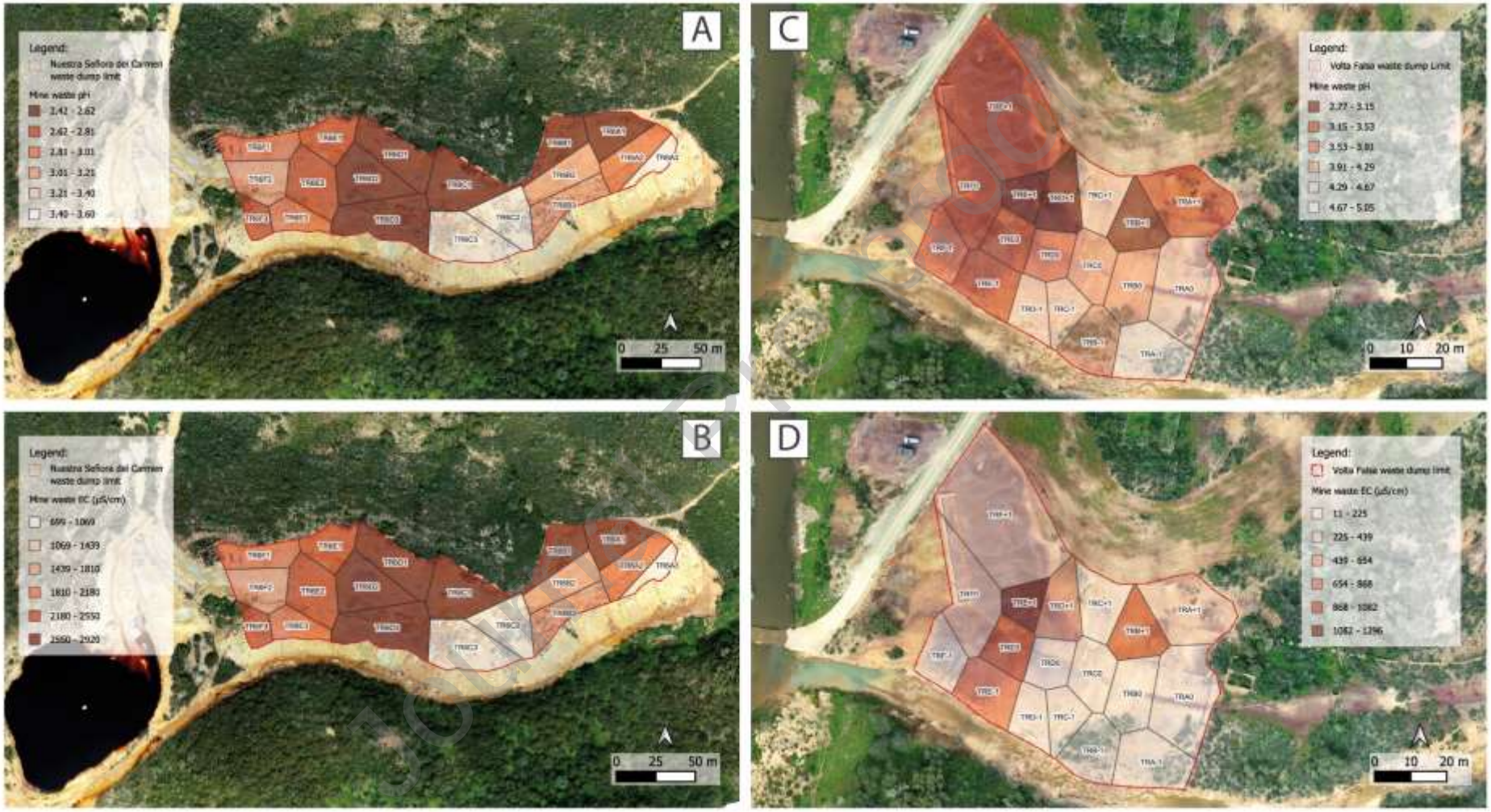


Figure 5. Spatial distribution of pH and EC parameters from mine wastes represented by Voronoi polygons on an orthomosaic, for two waste dumps: (A and B) NSC, and (C and D) VF.

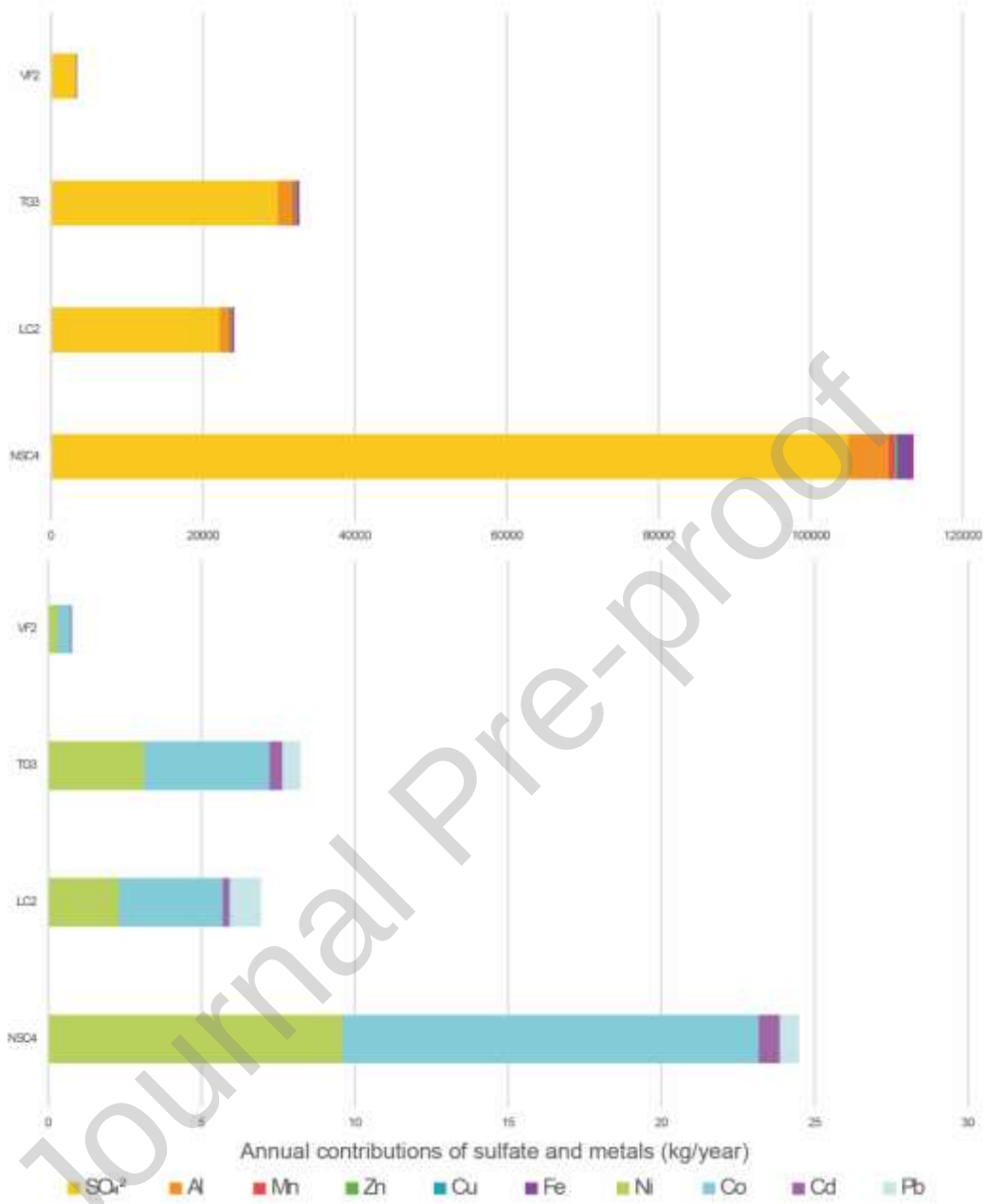


Figure 6. Annual contribution of sulfate and metals (kg/year) from each mine to the Trimpancho stream, which flows into Chança River.

6. Conclusion

This study provides a comprehensive assessment of the environmental effects of the Trimpancho mining complex, integrating UAV photogrammetry, water quality analysis, and mine waste characterization. The findings establish a clear connection between mine waste composition, topography, and water contamination, offering valuable insights for future monitoring and remediation efforts. Key findings and implications include:

- Water quality analysis confirms severe AMD, with low pH (2.59–8.27), high electrical conductivity (up to 4,171 µS/cm), and elevated metal concentrations (e.g., Fe = 65.7 mg/L, Al = 174 mg/L, Mn = 23.5 mg/L, Zn = 20.7 mg/L);

- Contaminant dispersion follows the Trimpancho stream, affecting the Chança River, a critical water resource for Portugal and Spain;
- Dilution effects in the Chança River reduce AMD severity, but contaminants persist, emphasizing the need for long-term water quality monitoring;
- Waste characterization reveals substantial differences in geochemical behavior between the NSC dump and the VF dump;
- The NSC dump (80% of total waste volume) contains highly reactive sulfides, leading to strong acid generation and metal leaching;
- The VF dump, composed mainly of slag and iron oxides, exhibits lower reactivity, contributing less to AMD formation;
- UAV-based slope analysis identifies highly erodible zones (>35° slopes), particularly around the NSC and LC waste dumps, where erosion accelerates metal and sulfate transport into water systems;
- Surface runoff modeling highlights key flow accumulation zones, reinforcing the link between topography and contaminant dispersion;
- UAV-derived photogrammetric analysis estimates a total waste volume of 253,377 m^3, with the NSC mine alone contributing 197,569 m^3;
- Geospatial analysis confirms that steep waste piles and uncontrolled disposal practices exacerbate erosion, AMD formation, and contaminant spread;
- UAV photogrammetry proves to be a cost-effective, high-resolution tool for waste volume estimation, erosion tracking, and hydrological mapping;
- The integration of remote sensing and field data provides a detailed spatial understanding of mine waste and flow dynamics, offering a scalable approach for monitoring other abandoned mining sites,

The study demonstrates the need for immediate intervention to stabilize highly reactive waste dumps (especially NSC) and prevent further AMD formation. Erosion control measures, such as vegetation cover and engineered barriers, should be implemented in steep slope areas to reduce contaminant transport. Long-term water quality monitoring along the Trimpancho and Chança rivers is essential to assess contaminant persistence and seasonal variations. Future research should focus on testing remediation strategies, such as passive AMD treatment systems, and evaluating their effectiveness in mitigating pollution.

This study also demonstrates the critical role of UAV-based monitoring in abandoned mining site management, providing detailed contamination assessment and practical insights for remediation planning. The findings contribute to the development of sustainable mine waste management strategies, ensuring better protection of water resources and ecosystems in historically mined regions.

Acknowledgments

Ana Barroso acknowledges FCT - Foundation for Science and Technology, I.P., by the support of ICT through the research fellowship with reference UI/BD/151330/2021. FCT also co-founded this work in the framework of the UIDB/04683– Instituto de Ciências da Terra programs. We are grateful to the reviewers for their valuable comments and suggestions, which helped to improve the manuscript.

Declaration of interest statement:

All authors have seen and approved the final version of the manuscript being submitted. They warrant that the article is the authors' original work, hasn't received prior publication and isn't under consideration for publication elsewhere.

References:

AEMET – Agencia Estatal de Meteorología 2024. Datos climatológicos. http://www.aemet.es (accessed 17 April 2025).

Alsayed, A., & Nabawy, M. R. (2023). Stockpile volume estimation in open and confined environments: a review. Drones, 7(8), 537. https://doi.org/10.3390/drones7080537

APHA Standard Methods for the Examination of Water and Wastewater, 20th ed.; (2012) American Public Health Association, American Water Works Association, Water Environment Federation: Washington, DC, USA.

Barriga, F. J. A. S. (1990). Metallogenesis in the Iberian pyrite belt. In Pre-mesozoic geology of Iberia (pp. 369-379). Berlin, Heidelberg: Springer Berlin Heidelberg.

Barroso, A., Mogo, S., Silva, M. M. V., Cachorro, V., & de Frutos, Á. (2021). Morphology, mineralogy, and chemistry of atmospheric aerosols nearby an active mining area: aljustrel mine (SW Portugal). Atmosphere, 12(3), 333. https://doi.org/10.3390/atmos12030333

Barroso, A., Valente, T., Marinho Reis, A. P., & Antunes, I. M. H. (2023). A new acidity-based approach for estimating total dissolved solids in acidic mining influenced water. Water, 15(16), 2995. https://doi.org/10.3390/w15162995

Beck, H. E., Zimmermann, N. E., McVicar, T. R., Vergopolan, N., Berg, A., & Wood, E. F. (2018). Present and future Köppen-Geiger climate classification maps at 1-km resolution. Scientific data, 5(1), 1-12. https://doi.org/10.1038/sdata.2018.214

Cánovas, C. R., González, R. M., Vieira, B. J., Waerenborgh, J. C., Marques, R., Macías, F., Basallote, M. D., Olias, M., Prudencio, M. I. (2023). Metal mobility and bioaccessibility from cyanide leaching heaps in a historical mine site. Journal of Hazardous Materials, 448, 130948. https://doi.org/10.1016/j.jhazmat.2023.130948

Cánovas, C. R., Macías, F., Basallote, M. D., Olías, M., Nieto, J. M., & Pérez-López, R. (2021). Metal (loid) release from sulfide-rich wastes to the environment: The case of the Iberian Pyrite Belt (SW Spain). Current Opinion in Environmental Science & Health, 20, 100240. https://doi.org/10.1016/j.coesh.2021.100240

Cánovas, C. R., Olías, M., Macias, F., Torres, E., San Miguel, E. G., Galván, L., Ayora, C., Nieto, J. M. (2016). Water acidification trends in a reservoir of the Iberian Pyrite Belt (SW Spain). Science of the Total Environment, 541, 400-411. https://doi.org/10.1016/j.scitotenv.2015.09.070

Cara, S., Fiori, M., & Matzuzzi, C. (2013, April). Assessment of landscape by photogrammetry proximity UAV survey technique: A case study of an abandoned mine site in the Furtei area (Sardinia-Italy). In *Proceedings of the 23rd International Mining Congress of Turkey* (pp. 83-91).

Carabassa, V., Montero, P., Alcañiz, J. M., & Padró, J. C. (2021). Soil erosion monitoring in quarry restoration using drones. Minerals, 11(9), 949. https://doi.org/10.3390/min11090949

Carvalho, D. D. (1979). Geologia, metalogenia e metodologia da investigação de sulfuretos polimetálicos do Sul de Portugal.

Da Silva, E. F., Fonseca, E. C., Matos, J. X., Patinha, C., Reis, P., & Santos Oliveira, J. M. (2005). The effect of unconfined mine tailings on the geochemistry of soils, sediments and surface waters of the Lousal area (Iberian Pyrite Belt, Southern Portugal). Land Degradation & Development, 16(2), 213-228. https://doi.org/10.1002/ldr.659

Dang, T. M., & Nguyen, B. D. (2023). Applications of UAVs in mine industry: A scoping review. Journal of Sustainable Mining, 22. https://doi.org/10.46873/2300-3960.1384

Davoise, D., & Méndez, A. Research of an Abandoned Tailings Deposit in the Iberian Pyritic Belt: Characterization and Gross Reserves Estimation. Processes 2023, 11, 1642. doi. org/10.3390/pr11061642. https://doi.org/10.3390/pr11061642

Doumas, P., Munoz, M., Banni, M., Becerra, S., Bruneel, O., Casiot, C., ... & Sappin-Didier, V. (2018). Polymetallic pollution from abandoned mines in Mediterranean regions: a

multidisciplinary approach to environmental risks. Regional environmental change, 18, 677-692. https://doi.org/10.1007/s10113-016-0939-x

Erguler, G. K., Erguler, Z. A., Akcakoca, H., & Ucar, A. (2014). The effect of column dimensions and particle size on the results of kinetic column test used for acid mine drainage (AMD) prediction. Minerals Engineering, 55, 18-29. https://doi.org/10.1016/j.mineng.2013.09.008

España, J. S., Pamo, E. L., Santofimia, E., Aduvire, O., Reyes, J., & Barettino, D. (2005). Acid mine drainage in the Iberian Pyrite Belt (Odiel river watershed, Huelva, SW Spain): geochemistry, mineralogy and environmental implications. Applied geochemistry, 20(7), 1320-1356. https://doi.org/10.1016/j.apgeochem.2005.01.011

Ficklin WH, Plumlee GS, Smith KS, McHugh JB (1992) Geochemicalclassification of mine drainages and natural drainages in miner-alized areas. In: Kharaka YK, Maest, AS (eds) Proceedings ofwater-rock interaction, Balkema, Rotterdan, no7, pp 381–384

Flores, H., Lorenz, S., Jackisch, R., Tusa, L., Contreras, I. C., Zimmermann, R., & Gloaguen, R. (2021). UAS-based hyperspectral environmental monitoring of acid mine drainage affected waters. *Minerals*, *11*(2), 182. https://doi.org/10.3390/min11020182

Fortes, J. C., Sarmiento, A. M., Luis, A. T., Santisteban, M., Davila, J. M., Córdoba, F., & Grande, J. A. (2021). Wasted Critical Raw Materials: A Polluted Environmental Scenario as potential source of economic interest elements in the Spanish part of the Iberian Pyrite Belt. *Water, Air, & Soil Pollution*, *232*, 1-9. https://doi.org/10.1007/s11270-021-05018-1

Gomes, P., & Valente, T. (2024). Seasonal impact of acid mine drainage on water quality and potential ecological risk in an old sulfide exploitation. Environmental Science and Pollution Research, 31(14), 21124-21135. https://doi.org/10.1007/s11356-024-32367-1

Gonçalves, J.A. and et Henriques, R. (2015) UAV Photogrammetry for Topographic Monitoring of Coastal Areas. ISPRS Journal of Photogrammetry and Remote Sensing, 104, 101-111. https://doi.org/10.1016/j.isprsjprs.2015.02.009

González, R. M., Olias, M., Macias, F., Cánovas, C. R., & de Villarán, R. F. (2018). Hydrological characterization and prediction of flood levels of acidic pit lakes in the Tharsis mines, Iberian Pyrite Belt. Journal of Hydrology, 566, 807-817. https://doi.org/10.1016/j.jhydrol.2018.09.046

Grande, J. A., Santisteban, M., Valente, T., de la Torre, M. L., & Gomes, P. (2017). Hydrochemical characterization of a river affected by acid mine drainage in the Iberian Pyrite Belt. Water Science and Technology, 75(11), 2499-2507. https://doi.org/10.2166/wst.2017.097

Hämmerle, M., Schütt, F., & Höfle, B. (2016). Terrestrial and unmanned aerial system imagery for deriving photogrammetric three-dimensional point clouds and volume models of mass wasting sites. *Journal of Applied Remote Sensing*, *10*(2), 026029-026029. https://doi.org/10.1117/1.JRS.10.026029

Helser, J., Vassilieva, E., & Cappuyns, V. (2022). Environmental and human health risk assessment of sulfidic mine waste: Bioaccessibility, leaching and mineralogy. Journal of Hazardous Materials, 424, 127313. https://doi.org/10.1016/j.jhazmat.2021.127313

Hoffert, J. R. (1947). Acid mine drainage. Industrial & Engineering Chemistry, 39(5), 642-646.

Inverno, C., Díez-Montes, A., Rosa, C., García-Crespo, J., Matos, J., García-Lobón, J. L., ... & Sousa, P. (2015). Introduction and geological setting of the Iberian Pyrite Belt. 3D, 4D and predictive modelling of major mineral belts in Europe, 191-208. https://doi.org/10.1007/978-3-319-17428-0_9

Isgró, M. A., Basallote, M. D., Caballero, I., & Barbero, L. (2022a). Comparison of UAS and sentinel-2 multispectral imagery for water quality monitoring: A case study for acid mine drainage affected areas (SW Spain). Remote Sensing, 14(16), 4053. https://doi.org/10.3390/rs14164053

Isgró, M. A., Basallote, M. D., & Barbero, L. (2022b). Unmanned aerial system-based multispectral water quality monitoring in the Iberian Pyrite Belt (SW Spain). *Mine Water and the Environment*, *41*(1), 30-41. https://doi.org/10.1007/s10230-021-00837-4

Jackisch, R., Lorenz, S., Zimmermann, R., Möckel, R., & Gloaguen, R. (2018). Drone-borne hyperspectral monitoring of acid mine drainage: An example from the Sokolov lignite district. *Remote sensing*, *10*(3), 385. **https://doi.org/10.3390/rs10030385**

Jahn, R., Blume, H. P., Asio, V. B., Spaargaren, O., & Schad, P. (2006). Guidelines for soil description. Fao. ISBN 9789251055212 – 97

Jakob, S., Zimmermann, R., & Gloaguen, R. (2017). The need for accurate geometric and radiometric corrections of drone-borne hyperspectral data for mineral exploration: Mephysto—A toolbox for pre-processing drone-borne hyperspectral data. *Remote Sensing*, *9*(1), 88. https://doi.org/10.3390/rs9010088

Keatley, A. C., Martin, P. G., Hallam, K. R., Payton, O. D., Awbery, R., Carvalho, F. P., ... & Scott, T. B. (2018). Source identification of uranium-containing materials at mine legacy sites in Portugal. *Journal of Environmental Radioactivity*, *183*, 102-111. https://doi.org/10.1016/j.jenvrad.2017.12.009

Leistel, J. M., Marcoux, E., Thiéblemont, D., Quesada, C., Sánchez, A., Almodóvar, G. R., Pascual, E., Saez, R. J. M. D. (1997). The volcanic-hosted massive sulphide deposits of the Iberian Pyrite Belt Review and preface to the Thematic Issue: Review and preface to the Thematic Issue. Mineralium deposita, *33*, 2-30. https://doi.org/10.1007/s001260050130

Lemos, M., Valente, T., Reis, P. M., Fonseca, R., Delbem, I., Ventura, J., & Magalhães, M. (2020). Mineralogical and geochemical characterization of gold mining tailings and their potential to generate acid mine drainage (Minas Gerais, Brazil). Minerals, 11(1), 39. https://doi.org/10.3390/min11010039

León, R., Macías, F., Cánovas, C. R., Pérez-López, R., Ayora, C., Nieto, J. M., & Olías, M. (2021). Mine waters as a secondary source of rare earth elements worldwide: The case of the Iberian Pyrite Belt. Journal of Geochemical Exploration, 224, 106742. https://doi.org/10.1016/j.gexplo.2021.106742

Martín-Velázquez, S., Rodríguez-Santalla, I., Ropero-Szymańska, N., Gomez-Ortiz, D., Martín-Crespo, T., & de Ignacio-San José, C. (2022). Geomorphological mapping and erosion of abandoned tailings in the hiendelaencina Mining District (Spain) from Aerial Imagery and LiDAR Data. Remote Sensing, 14(18), 4617. https://doi.org/10.3390/rs14184617

Moreno Gonzalez, R., Barbero, L., Curcio, A. C., León, R., and Romero, J.: Assessment of pollutant load in Tharsis mine (Huelva, Spain): A study of evaporitic salts using UAS-Based Hyperspectral, EGU General Assembly 2024, Vienna, Austria, 14–19 Apr 2024, EGU24-20817, https://doi.org/10.5194/egusphere-egu24-20817, 2024.

Nocete, F., Sáez, R., Nieto, J. M., Cruz-Auñón, R., Cabrero, R., Alex, E., & Bayona, M. R. (2005). Circulation of silicified oolitic limestone blades in South-Iberia (Spain and Portugal) during the third millennium BC: an expression of a core/periphery framework. Journal of Anthropological Archaeology, 24(1), 62-81. https://doi.org/10.1016/j.jaa.2004.10.002

Nogueira, P., Silva, M., Roseiro, J., Potes, M., & Rodrigues, G. (2023). Mapping the Mine: Combining Portable X-ray Fluorescence, Spectroradiometry, UAV, and Sentinel-2 Images to Identify Contaminated Soils—Application to the Mostardeira Mine (Portugal). Remote Sensing, 15(22), 5295. https://doi.org/10.3390/rs15225295

Nordstrom, D. K. (2011). Mine waters: acidic to circmneutral. Elements, 7(6), 393-398. https://doi.org/10.2113/gselements.7.6.393

Olías, M., Cánovas, C. R., Macías, F., Basallote, M. D., & Nieto, J. M. (2020). The evolution of pollutant concentrations in a river severely affected by acid mine drainage: Río Tinto (SW Spain). Minerals, 10(7), 598. https://doi.org/10.3390/min10070598

Olías, M., Nieto, J. M., Pérez-López, R., Cánovas, C. R., Macías, F., Sarmiento, A. M., & Galván, L. (2016). Controls on acid mine water composition from the Iberian Pyrite Belt (SW Spain). Catena, 137, 12-23. https://doi.org/10.1016/j.catena.2015.08.018

Olıas, M., Nieto, J. M., Sarmiento, A. M., Cerón, J. C., & Cánovas, C. R. (2004). Seasonal water quality variations in a river affected by acid mine drainage: the Odiel River (South West Spain). Science of the total environment, 333(1-3), 267-281. https://doi.org/10.1016/j.scitotenv.2004.05.012

Ostalé, E. P. (2014). Caracterización ambiental de estructuras mineras en la Faja Pirítica Ibérica como soporte metodológico de gestión territorial (Doctoral dissertation, Universidad de Huelva).

Padró, J. C., Cardozo, J., Montero, P., Ruiz-Carulla, R., Alcañiz, J. M., Serra, D., & Carabassa, V. (2022). Drone-based identification of erosive processes in open-pit mining restored areas. Land, 11(2), 212. https://doi.org/10.3390/land11020212

Park, S., & Choi, Y. (2020). Applications of unmanned aerial vehicles in mining from exploration to reclamation: A review. Minerals, 10(8), 663. https://doi.org/10.3390/min10080663

Parviainen, A., Rosca, C., Rondon, D., Porcel, M. C., & Martín-Peinado, F. J. (2024). Assessment of atmospheric pollution by potentially toxic elements in the urban areas of the Riotinto mining district. Chemosphere, 363, 142906. https://doi.org/10.1016/j.chemosphere.2024.142906

Quental, L., Gonçalves, P., Oliveira, D. P., Batista, M. J., Matos, J. X., Sousa, A. J., ... & Dias, R. P. (2020). Multispectral and hyperspectral remote sensing as a source of knowledge in the Portuguese sector of the Iberian Pyrite Belt. *Comunicações Geológicas*, *107*(Especial III), 21-39. DOI: 10.34637/7ypw-gm88

Rauhala, A., Tuomela, A., Davids, C., & Rossi, P. M. (2017). UAV remote sensing surveillance of a mine tailings impoundment in sub-arctic conditions. *Remote sensing*, *9*(12), 1318. **https://doi.org/10.3390/rs9121318**

Sánchez-Donoso, R., Martín-Duque, J. F., Crespo, E., & Higueras, P. L. (2019). Tailing's geomorphology of the San Quintín mining site (Spain): landform catalogue, aeolian erosion and environmental implications. Environmental Earth Sciences, 78, 1-17. https://doi.org/10.1007/s12665-019-8148-9

Sánchez-Donoso, R., García Lorenzo, M. L., Esbrí, J. M., García-Noguero, E. M., Higueras, P., & Crespo, E. (2021). Geochemical characterization and trace-element mobility assessment for metallic mine reclamation in soils affected by mine activities in the iberian pyrite belt. Geosciences, 11(6), 233. https://doi.org/10.3390/geosciences11060233

Sims, D. B., Hooda, P. S., & Gillmore, G. (2013). Mining activities and associated environmental impacts in arid climates: a literature review. Environment and Pollution, 2(4), 22-43. http://dx.doi.org/10.5539/ep.v2n4p22

Tong, X., Liu, X., Chen, P., Liu, S., Luan, K., Li, L., ... & Hong, Z. (2015). Integration of UAV-based photogrammetry and terrestrial laser scanning for the three-dimensional mapping and monitoring of open-pit mine areas. *Remote Sensing*, *7*(6), 6635-6662. **https://doi.org/10.3390/rs70606635**

Tornos, F. (2006). Environment of formation and styles of volcanogenic massive sulfides: The Iberian Pyrite Belt. Ore Geology Reviews, 28(3), 259-307. https://doi.org/10.1016/j.oregeorev.2004.12.005

Tornos, F., Barriga, F. J. A. S., Marcoux, E., Pascual, E., Pons, J. M., Relvas, J. M. R. S., ... & Blundell, D. (2000). The Iberian pyrite belt. Database on Global VMS Districts, Codes-Geode, 19-52.

Xiang, J., Chen, J., Sofia, G., Tian, Y., & Tarolli, P. (2018). Open-pit mine geomorphic changes analysis using multi-temporal UAV survey. *Environmental earth sciences*, *77*, 1-18. https://doi.org/10.1007/s12665-018-7383-9

Journal Pre-proof

Environmental implication (maximum of 100 words):

This study highlights the severe environmental impacts of abandoned mine waste in the Iberian Pyrite Belt. High sulfide content and steep slopes contribute to acid mine drainage, contaminating downstream water bodies, including the Chança River. UAV-based photogrammetry combined with hydrochemical data revealed critical hotspots for contaminant mobilization. These insights are essential for prioritizing remediation strategies and guiding sustainable management of legacy mining sites, especially in transboundary water systems at risk.

The authors declare that they have no known competing financial interests or personal relationships that could have appeared to influence the work reported in this paper



Highlights:

- AMD confirmed, with pH as low as 2.59 and high metal concentrations and loads.
- Erosion hotspots on slopes >30° increase metal transport to water bodies.
- NSC dump shows higher leaching potential than VF, mainly slag and oxides.
- UAV Photogrammetry enables high-resolution mapping of waste and drainage patterns.
- Multi-method approach enhances monitoring, highlighting priority areas for AMD mitigation.

Journal Pre-proof